Mikrochim. Acta 116, 1– 31 (1994)

Mikrochimica Acta

Fundamental Review

Characterization of Polymer Materials by Scattering Techniques, with Applications to Block Copolymers

Tim Lodge

Department of Chemistry, University of Minnesota, Minneapolis, MN 55455-0431, U.S.A.

Abstract. The application of six techniques—static and dynamic light scattering, small-angle neutron and X-ray scattering, neutron and X-ray reflectivity—to the characterization of polymer materials is summarized. Emphasis is placed on the similarities and differences among the various techniques, and on recent advances in experimental practice. Twelve examples from the recent literature are described, most of which concern block copolymers. A brief introduction to block copolymer properties is also provided.

Key words: block copolymers, light scattering, neutron scattering, X-ray scattering.

Contents

I. Introduction

The complete molecular characterization of a polymeric material requires a broad spectrum of analytical techniques. Information of interest for a given sample might

include average molecular weight, molecular weight distribution, stereochemistry, copolymer composition, branching, overall molecular size and shape, mobility, and conformational relaxation times. As challenging a task as this may be in dilute solution, it is often desirable to obtain some of this information in situ, such as in a bulk material or thin film. For example, many useful polymeric materials are insoluble; alternatively, it may be the molecular properties in the bulk material that are of most importance, such as the spatial distribution in a composite. In either the solution or bulk case, scattering techniques have proven to be an essential component of the analytical armamentarium.

Scattering experiments provide a non-invasive probe of structure, interactions, and dynamics over lengthscales from 1 nm to 10 μm, and timescales from nanoseconds to hours. Light, neutrons, and X-rays are the three forms of radiation relevant for polymer characterization. Each exhibits unique features that render the three approaches complementary, but the underlying physics is sufficiently similar that all may be considered together. Although the basic techniques are well-established, there have been several recent developments in experimental practice that significantly enhance the kind of information that may be obtained, and/or the ease with which it may be extracted.

In this article, the basic phenomena underlying scattering experiments are reviewed, and the principal differences among the three techniques are highlighted. Specific experiments discussed include total intensity light scattering (LS), dynamic light scattering (DLS), small-angle neutron scattering (SANS), small-angle X-ray scattering (SAXS), neutron reflection (NR), and X-ray reflection (XR). Twelve examples from the recent literature have been chosen to demonstrate some of the more interesting applications. To provide thematic continuity, most of the examples selected concern scattering from block copolymers. Block copolymers constitute a technologically important and scientifically fascinating class of materials, and provide excellent illustrations of the power of scattering techniques. However, this article should not be construed as a thorough review of scattering from polymers in general, or scattering from block copolymers in particular. Rather, it provides a self-contained summary of scattering techniques designed for the analytical chemistry community; the emphasis is on the kinds of information that can be obtained, the similarities and differences among the techniques, and recent developments in experimental practice. More detailed treatments of the various techniques can be found as follows: LS [1, 2], DLS [3–5], SANS [6, 7], NR [8, 9], SAXS [10, 11], and XR [8].

II. Fundamentals of Scattering

The basic scattering experiment is illustrated in Fig. 1. An unpolarized incident wave ($\psi_o \exp[i\omega t - \mathbf{k}_i \cdot \mathbf{r}]$) with intensity I_o enters the material, and the scattered wave ($\psi_s \exp[i\omega t - \mathbf{k}_f \cdot \mathbf{r}]$) with intensity I_s is detected at an angle θ. We restrict ourselves to elastic scattering, such that incident and scattered waves have the same energy ($h\omega$), but the change in direction necessarily represents a change in momentum. This is quantified by the momentum transfer vector, $\mathbf{q}$, defined as

$$q = |\mathbf{q}| \equiv |\mathbf{k}_i - \mathbf{k}_f| = \left(\frac{4\pi}{\lambda}\right) \sin\left(\frac{\theta}{2}\right), \tag{1}$$

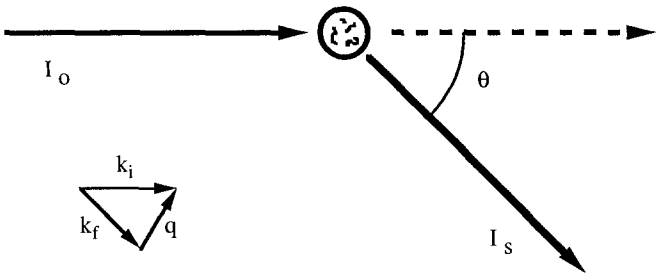

Fig. 1. Schematic illustration of a scattering experiment

where $|\mathbf{k}| = (2\pi/\lambda)$ and λ is the wavelength in the material. In any experiment, $I_s(q)/I_o$ is determined by the product of three factors: the amplitude of the mean square concentration fluctuations, the spatial correlations among the fluctuations, and a contrast factor. The first of these indicates that we are considering only molecular mixtures, and that scattering due to fluctuations in density, temperature, etc., may be ignored (or easily subtracted); this is not a particularly restrictive assumption.

Consider an absolutely regular and uniform array of scattering centers (e.g., atoms or molecules) with a characteristic spacing r_{ij}, and an incident beam with $\lambda \gg r_{ij}$. The scattered intensity at any $q \neq 0$ will be zero, because for every scatterer, one can always find another that is $\lambda/2$ further from the detector, resulting in complete destructive interference. However, if a few scatterers are removed from the array at random, this complete "pairing off" will break down, and I_s will no longer be zero; thus, scattering is caused by *fluctuations* in composition. In this instance, I_s will be independent of q, because there is no preferred distance, or spatial correlation, among the fluctuations; such scattering is termed *incoherent*. Returning to the original perfect array, let λ be reduced such that $\lambda \approx r_{ij}$. In this case, perfect constructive interference will occur at selected (and narrowly-defined) values of q: this is Bragg diffraction. For an amorphous material exhibiting partial spatial correlations among the scattering centers, I_s will be a smoothly varying function of q. Thus, it is order on the lengthscale of $2\pi/q$ that gives rise to *coherent*, or angle-dependent scattering. The third factor identified above, the contrast, quantifies the degree to which a given composition fluctuation modulates the appropriate material parameter: dielectric constant (refractive index) for light, scattering cross section for neutrons, electron density for X-rays.

The mean square composition fluctuation in an equilibrium binary mixture, $\langle(\delta c)^2\rangle$, is determined by the free energy penalty associated with such fluctuations:

$$\langle(\delta c)^2\rangle = \frac{ckT}{(\partial^2 \Delta G_{mix}/\partial c^2)} = \frac{ckT}{(\partial \Pi/\partial c)}, \tag{2}$$

where $\partial\Pi/\partial c$ is the osmotic compressibility and ΔG_{mix} is the free energy of mixing. Eq. (2) illustrates the fact that scattering provides thermodynamic information. The interference among waves scattered from different centers is obtained by simple superposition:

$$\Psi_s(q) = \sum_j \psi_{s,j} \exp[i(\omega t - \mathbf{q}\cdot\mathbf{r}_j)], \tag{3}$$

where the index j runs over all the scatterers in the scattering volume, and $\psi_{s,j}$ depends on j only if the different scatterers have a different scattering power, b_j. The

scattered intensity is given by

$$\frac{I_s(q)}{I_o} = \frac{\langle \Psi_s(q)\Psi_s^*(q)\rangle}{\langle \Psi_o\Psi_o^*\rangle} \propto \sum_j \sum_k \langle b_j b_k^* \exp[-i\mathbf{q}\cdot\mathbf{r}_{jk}]\rangle, \tag{4}$$

where $\mathbf{r}_{jk} = \mathbf{r}_j - \mathbf{r}_k$. This double sum, normalized by N^2, the square of the number of scatterers in the sample volume, defines the static structure factor, S(q):

$$S(q) \equiv \frac{1}{N^2} \sum_j^N \sum_k^N \langle b_j b_k^* \exp[-i\mathbf{q}\cdot\mathbf{r}_{jk}]\rangle. \tag{5}$$

The average $\langle \cdots \rangle$ is taken over the pair correlation function $g(\mathbf{r}_{jk})$, i.e., the joint probability that scatterer j is located at $\mathbf{r}_j$ and scatterer k is located at $\mathbf{r}_k$. Eq. (5) contains the spatial Fourier transform of $g(\mathbf{r}_{jk})$, which illustrates why a scattering experiment can be said to provide a Fourier image of the sample structure. If the temporal fluctuations in the positions of the scatterers are considered, one obtains the dynamic structure factor, S(q, t):

$$S(q,t) \equiv \frac{1}{N^2} \sum_j^N \sum_k^N \langle b_j b_k^* \exp[-i\mathbf{q}\cdot(\mathbf{r}_j(t) - \mathbf{r}_k(0))]\rangle \tag{6}$$

From Eqs. (5) and (6), and the prior arguments based on the perfect array of scatterers, it should be clear that it is *differences* between the values of b_j and b_k that matter most; if all the b_j are the same, only density fluctuations will contribute to scattering. Consider two examples. For a dilute polymer solution, the solvent provides a featureless background, but will still scatter through density fluctuations; the intensity scattered by the solution, minus the intensity from the pure solvent, is termed the excess scattering. Each monomer on a polymer has the same b, and thus S(q) or S(q, t) from the excess scattering reflects the structure and dynamics of the polymer. Note that the sums in Eqs. (5) and (6) should be taken over the scattering volume, which contains many polymer molecules. Thus, even in dilute solution the measured intensity will reflect both intrachain and interchain contributions. The latter are taken into account via Zimm's "single-contact approximation", and extrapolation to infinite dilution [1, 2, 12]. As a second example, consider a blend of two polymers in the molten state. Here, the total structure factors can be resolved into composition-weighted single chain structure factors, plus a contribution from the interchain terms. In the framework of mean-field theory, the interchain contribution can be expressed as a function of the single chain terms, via the so-called "random phase approximation" [13]. This permits extraction of single chain information without taking the infinite dilution limit.

Given that composition fluctuations are a property of the material, the principal distinctions among the various scattering techniques lie in the range of q, and the nature of b_j. A typical light scattering experiment ($350 \leq \lambda_o \leq 700$ nm; $30° \leq \theta \leq 150°$) covers the range $0.0007 \leq q^{-1} \leq 0.005$ Å^{-1} (assuming the refractive index in the material is ca. 1.5), corresponding to correlations on the lengthscale of 10^2–10^4 Å. Instruments with angular resolution down to 5° and below have also been constructed. Both neutrons and X-rays employ radiation with $1 \leq \lambda \leq 10$ Å, and consequently are appropriate for smaller scale structures. However, the angular resolution in these experiments is also greater; for example, in SANS θ values of 0.05° are accessible, so that the typical q range of 0.005 to 0.1 Å^{-1} can virtually

overlap with light scattering. The combined range thus spans the relevant size scales for most polymer systems.

For light scattering from composition fluctuations, b_j is proportional to the refractive index increment, $(\partial n/\partial c)_j$. In general, therefore, one seeks polymer/solvent or polymer/polymer pairs which have substantial differences in refractive index. For neutron scattering, b_j is the coherent scattering length of the nucleus, a property with a component that varies seemingly randomly across the periodic table. Notably, ^1H and ^2H have very different coherent scattering lengths, a fact that underlies almost all applications of neutron scattering to polymer systems. Selective deuterium labelling thus permits examination of S(q) for single chains, or even parts of chains, in solution or in the bulk; the thermodynamic effect of isotopic substitution is usually (but not always) negligible. One complication with neutrons is the presence of an incoherent scattering cross section, $(4\pi b_j^2)_{inc}$, for nuclei with non-zero spin I, due to the differences in scattering length for nucleus-neutron pairs with net spin $I + 1/2$ and $I - 1/2$ (neutrons have spin 1/2). This results in a q-independent background intensity, particularly in systems with many ^1H atoms. For x-rays, b_j increases monotonically with atomic number, which favors applications to systems with heavy atoms. However, even amorphous hydrocarbons can give substantial scattered intensity when the concentration fluctuations are large.

III. Block Copolymers

A copolymer is a polymer incorporating two or more monomer units (A, B, C ...); in a block copolymer, the different monomers are grouped sequentially (AAA ... BBB ... CCC ...). The most commonly employed architectures are diblocks $(A)_n(B)_m$ and symmetric triblocks $(A)_n(B)_m(A)_n$, where the indicies n and m denote the degrees of polymerization, but many more elaborate topologies have been synthesized. The driving force behind the application of block copolymers is their inherently composite nature: they provide a means to incorporate different physical properties into a single molecule, and thereby circumvent the macroscopic phase separation that usually accompanies attempts to blend chemically different homopolymers. For example, a small amount of an AB diblock can stabilize a blend of immiscible A and B polymers, thereby acting as a macromolecular surfactant. Alternatively, in the pure block copolymer, the thermodynamic repulsion between monomers drives the system to self-assemble into one of an interesting variety of morphologies; the resulting order-disorder transition (ODT), or microphase separation transition, is a topic of considerable current research interest [14–16]. Examples of the observed morphologies are illustrated in Fig. 2. For a given diblock copolymer, the selection of morphology, or equivalently, the phase diagram, depends on N, the total degree

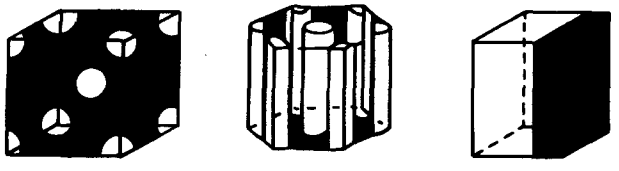

Fig. 2. Three commonly observed block copolymer morphologies: a body-centered cubic array of spheres; a hexagonal array of cylinders; lamellae

of polymerization; $f_A = N_A/(N_A + N_B)$, the fractional composition; and χ, the A-B interaction parameter ($\chi \sim T^{-1}$). Recently, it has become apparent that other variables are also important; the leading candidate is a_A/a_B, where a is the statistical segment length of the block [17].

The various morphologies in Fig. 2 offer some intriguing possibilities from the perspective of nanostructured materials. In each case, the characteristic dimensions of the structure are governed by the dimensions of individual chains, and are thus subject to synthetic control; they typically lie in the 50–500 Å range. For example, in the lamellar case, the period is roughly 4 R_g, where R_g is the radius of gyration of the polymer, as shown in Fig. 3. In each microstructure, the average end-to-end

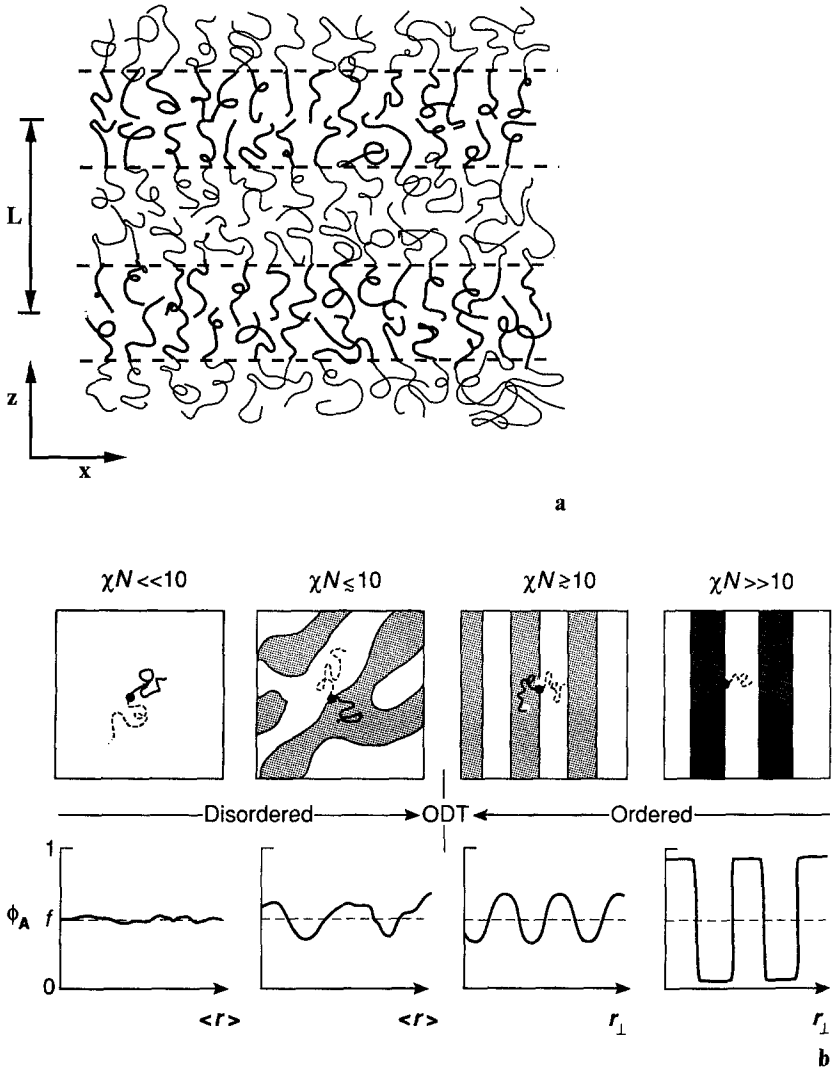

Fig. 3. Schematic illustration of block copolymer chains in a lamellar morphology: **a** the chain junctions reside preferentially in the interfacial zone, and the individual blocks are stretched away from the interface; **b** the composition profiles as a function of χN are also illustrated, including the fluctuation regime on the disordered side of the ODT. Reproduced, with permission, from [16]

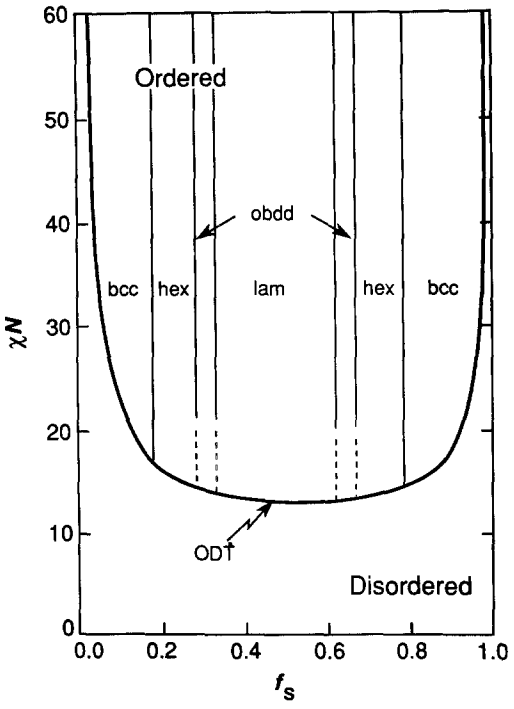

Fig. 4. A schematic phase diagram for diblock copolymers, based on the mean-field theory with fluctuations [18, 19], reproduced from [16]. The experimental phase diagram is considerably more complex, particularly in the vicinity of the order-disorder transition (ODT). In addition, the ordered bicontinuous double diamond (*obdd*) phase is currently undergoing re-examination

vector of an individual chain lies normal to the interface between microdomains, and the chain junctions (i.e., the covalent A-B linkages) tend to be confined to the interfacial zone. Some of the microstructures are inherently anisotropic (e.g., lamellar and cylindrical), whereas others are isotropic (e.g., cubic). Similarly, some are bicontinuous, some continuous in one component, and the lamellar phase is not necessarily continuous (in three dimensions) in either component. Presumably, the various structures represent free energy minima, which is advantageous from a processing perspective. As polymeric materials, such structures also have the typical advantages of low density, mechanical strength and/or flexibility, and relative cost-effectiveness. Although block copolymers already enjoy considerable commercial importance, the overall trend toward tailored materials promises an increasing role for multicomponent polymers in general.

To underscore the complexity of block copolymer behavior, consider the schematic phase diagram for A-B diblocks shown in Fig. 4 [16, 18, 19]. This figure is based on the mean-field model of Leibler [18], modified to account for fluctuation contributions [19]. To a first approximation, the ODT (shown as the solid curve) is determined by the dimensionless product χN, as a function of f_A; χ determines the enthalpic part of the free energy, and the entropy of mixing for polymers scales as N^{-1}. For a symmetric diblock ($f = 1/2$), the ODT occurs near $\chi N = 10.5$. Within the ordered state, the dashed lines indicate approximate boundaries between different morphologies, or order-order transitions (OOTs). Particularly near the ODT, these lines are not vertical, indicating that one may expect to observe OOTs for a single sample, just by varying T. Even for $f = 1/2$, the structure evolves as χN is increased within the ordered state. For example, near the ODT, in the so-called "weak-segregation regime", the composition profiles in space are expected to be

sinusoidal, as illustrated in Fig. 3. The interfacial zones, therefore, are very broad. As χN increases, so does the enthalpic penalty for A-B contacts, and the composition profiles sharpen toward a square wave (actually a hyperbolic tangent function). To accommodate this change, while maintaining bulk density, the individual chains stretch away from the interface, and the lamellar period, L, increases. This stretching leads to a characteristic $L \sim N^{0.67}$ scaling, in contrast to the $L \sim N^{0.5}$ associated with unperturbed ("Gaussian") chains.

Even on the disordered side of the ODT, the behavior of block copolymers is quite interesting. Within a region near the ODT, there is evidence of large amplitude composition fluctuations [20], in at least qualitative agreement with theory [19], and "polarization", or stretching of the individual chains beyond their disordered melt conformations [21], as will be discussed subsequently. These fluctuations are reminiscent of critical fluctuations in a binary mixture near the spinodal, but the block copolymer case is different in two respects. First, the wavelength of the fluctuations is still pinned by R_g, so there is no "critical opalescence" due to a diverging correlation length. Second, the fluctuation window is very broad, extending tens of degrees away from the T_{ODT}. Consequently, these fluctuations are of more than academic interest. The reason for this broad window, and the individual chain stretching, is related to the fact that the two blocks are, in a sense, frustrated; if the two blocks were isolated homopolymers, they would have phase separated macroscopically when $\chi N \approx 4$.

IV. Scattering Techniques and Recent Applications

A. Static Light Scattering (LS)

The LS experiment has been used for almost fifty years to examine polymers in dilute solution [22, 23], and commercial instruments have been available since the 1950s. At low polymer concentrations, the expression for the mean square fluctuations given in Eq. (2) can be expanded as

$$\langle (\delta c)^2 \rangle = \frac{ckT}{(M^{-1} + 2A_2c + 3A_3c^2 + \cdots)}, \tag{7}$$

where A_2 and A_3 are the second and third virial coefficients, respectively. For a good solvent, A_2 is positive, denoting an effective repulsion between chains; for a poor solvent, A_2 is negative, and at one particular temperature, the Flory "theta" temperature, $A_2 = 0$. Similarly, at low values of qR_g, where R_g is the radius of gyration of the polymer (R_g^2 is the second moment of the monomer distribution function), and in the limit of infinite dilution, the structure factor reduces to the form factor for an isolated chain, P(q), which can be expanded as

$$P(q) = 1 - \frac{(qR_g)^2}{3} + \cdots. \tag{8}$$

These results may be combined to give the equation:

$$\frac{Kc}{R_\theta} = \frac{1}{MP(q)} + 2A_2c + \cdots = \frac{\{1 + (qR_g)^2/3 + \cdots\}}{M} + 2A_2c + \cdots, \tag{9}$$

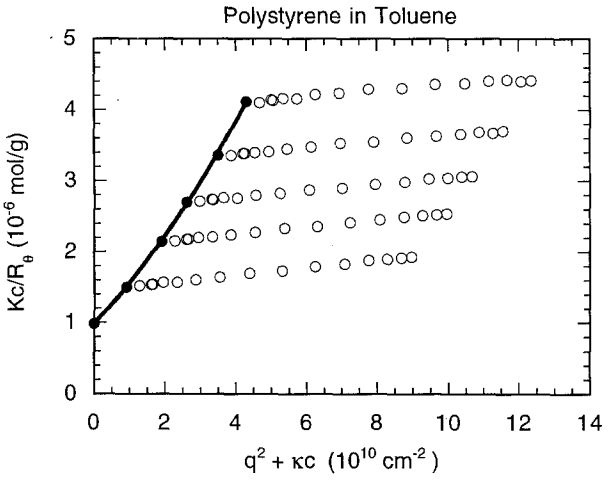

Fig. 5. Zimm plot for PS in toluene. The resulting values of M_w, A_2, and R_g are 9.9×10^5 g/mol, $2.1_2 \times 10^{-4}$ ml mol/g^2, and 396 ± 20 Å, respectively

where K is a collection of constants, including $(\partial n/\partial c)^2$, and R_θ is the Rayleigh ratio:

$$R_\theta(q) \equiv \frac{I_s(q)_{solution} - I_s(q)_{solvent}}{I_o(1 + \cos^2\theta)r^{-2}}. \tag{10}$$

The $\cos^2\theta$ term is appropriate for unpolarized incident light, and r is the sample to detector distance. Eq. (9) suggests a double extrapolation of the data to zero c and zero q, the so-called Zimm plot. An example is shown in Fig. 5, for a high molecular weight polystyrene fraction in toluene [24]. Data were obtained at 14 angles and for 5 concentrations. The constant, κ, on the ordinate is chosen in order to spread the data out appropriately. The open symbols correspond to the actual data, and the closed symbols to the corresponding values extrapolated to q = 0. The quantities of interest, M_w, R_g, and A_2, are determined from the joint intercept and the limiting slopes of the c = 0 and q = 0 extrapolated data, respectively; note that it is the weight average molecular weight and the z-average radius of gyration that are determined for a polydisperse sample. In this data set, the concentrations selected were such that the A_3 terms in Eq. (9) are significant. Consequently, the extrapolations to c = 0 (not shown on the plot) are not linear. In fact, for the q = 0 extrapolated data, one can discern the positive curvature with increasing concentration, reflecting a positive A_3.

LS has the advantage of providing an absolute measurement of M_w, provided that $\partial n/\partial c$ is known, and, in an instrument with angular resolution, an absolute measurement of R_g. This has recently been exploited with the development of LS as a detector in size exclusion chromatography (SEC). SEC is the premier technique for routine analysis of molecular weight and molecular weight distribution, but it is a relative technique only. Furthermore, the separation is based on hydrodynamic volume ($\sim R_g^3$), so it is desirable to have independent measurements of M and R_g. For example, a series of branched polymers of identical M could have widely varing R_g, and thus elution volumes. The Chromatix KMX-6 was the first commercial LS detector for SEC, but could only provide measurements over a narrow angular range ($< 10°$) [25]. More recently, Wyatt Technology has developed the DAWN instrument, in which roughly 15 photodiodes surround the sample volume, and the highly collimated laser beam is directed along the axis of the SEC elution capillary

[26]. In essence, this instrument can provide quasi-instantaneous Zimm plots all along the elution curve. The data in Fig. 5 were acquired with a DAWN photometer, albeit not in the flow mode. Assessments and comparisons of commercial light scattering photometers have recently appeared [27].

Example 1. Application of LS is not restricted to measurements of M_w, R_g, and A_2 in very dilute solutions. For example, by using a technique called contrast matching, it has proven possible to determine R_g for a tracer polymer present in a concentrated solution of another, chemically different matrix polymer [28]. Contrast matching in this case means to select the solvent, temperature, and wavelength such that $\partial n/\partial c = 0$ for the matrix polymer; the excess scattering is thus attributable directly to the tracer. This is not a completely general approach, in that all the appropriate conditions may be hard to satisfy concurrently. Furthermore, it is important that $\partial n/\partial c$ for the matrix be extremely close to zero, if the matrix polymer concentration is substantial, else significant errors may result, as discussed recently [29, 30]. An example of the application of contrast matching to block copolymers is shown in Fig. 6, for a polystyrene (PS)-poly(methylmethacrylate) (PMMA) diblock copolymer [24, 31]. The solvent, ethyl benzoate, is good for both components, and exactly index matches PMMA at 15°C for $\lambda_0 = 633$ nm, so that R_g for the PS block could be determined. The question of interest is whether the repulsive interaction between the PS and PMMA blocks causes an expansion of the PS block relative to a PS homopolymer of the same molecular weight, in the same solvent. This has been an issue of some past controversy, but these results, in agreement with the most detailed previous examinations [29], suggest that there is no significant extra expansion. (Note that there may be some expansion, due to the fact that the total swelling of a homopolymer in a good solvent increases with total molecular weight). Another interesting feature in Fig. 6 is the strong negative curvature in the $q = 0$ extrapolated data; this indicates that A_3 is negative, in contrast to the homopolymer case.

Example 2. LS has also been used to examine morphology and the time evolution of structure in polymer blends. These instruments have become practical with the advent of one- and two-dimensional detectors, such as photodiode arrays and

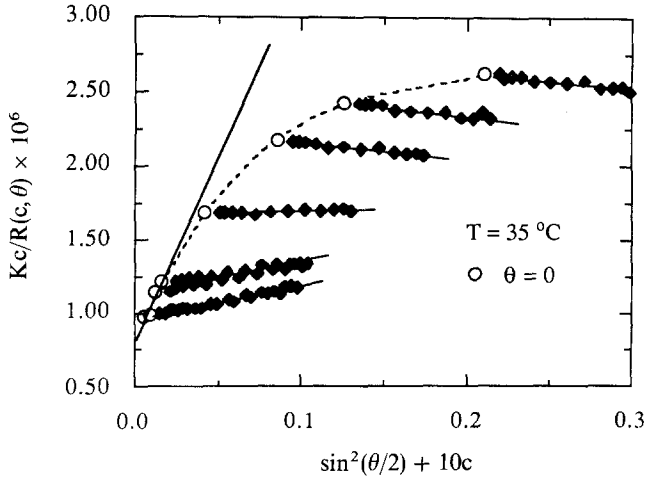

Fig. 6. Zimm plot for a PS-PMMA block copolymer in ethyl benzoate. The solvent is isorefractive with the PMMA block, and R_g for the PS block ($M_w = 3.1 \times 10^5$) was determined to be 322 ± 30 Å

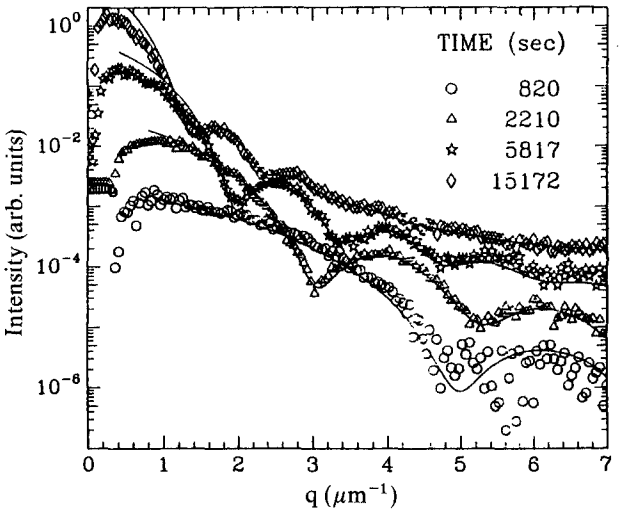

Fig. 7. Scattered intensity as a function of time after a quench into the metastable region, for a PI/PEP blend. The smooth curves correspond to the form factor for an isolated sphere, smeared for a small but finite polydispersity. Reproduced, with permission, from [33]

charge-coupled device cameras, whereby the angular dependence of I_s can be determined very quickly in non-equilibrium samples [32, 33]. An example is shown in Fig. 7, for a blend of polyisoprene (PI) and its fully saturated analog, poly(ethyleneepropylene) (PEP) [33]. This minor difference in chemical structure is quite sufficient to drive phase separation, for sufficiently high molecular weights. The blend was quenched into the metastable regime (between the binodal and spinodal), resulting in phase separation by a nucleation and growth process. Interestingly, the early growth process produced spheres that were very narrowly distributed in size (breadth $\approx 3\%$), due presumably to rapid heterogeneous nucleation at a fixed number of sites. Consequently, $I_s(q)$ displayed the multiple peaks associated with the structure factor for an isolated sphere. Note that partial deuteration was sufficient to provide ample scattered intensity; although $\partial n/\partial c$ is small, c is high. Indeed, in blends of polymers with distinctly different refractive indices, multiple scattering becomes a serious concern.

B. Dynamic Light Scattering (DLS)

In DLS, or "quasi-elastic" light scattering, the temporal fluctuations in I_s are monitored [3–5]; these fluctuations reflect changes in the spatial arrangement of scatterers, through S(q, t) defined in Eq. (6). Specifically, one is interested in the normalized time autocorrelation function of the scattered electric field, $E_s(t)$:

$$g^{(1)}(q, t) = \frac{\langle E_s(\tau)E_s^*(t+\tau)\rangle}{\langle |E_s(\tau)|^2\rangle} = \frac{1}{\langle |E_s(\tau)|^2\rangle} \lim_{T\to\infty}\left(\frac{1}{T}\right)\int_0^T E_s(\tau)E_s^*(t+\tau)\,d\tau, \quad (11)$$

and thus from Eqs. (3–6)

$$g^{(1)}(q, t) = \frac{S(q, t)}{S(q, 0)}. \quad (12)$$

Experimentally, one determines the autocorrelation function of the scattered intensity,

$$g^{(2)}(q, t) = \frac{\langle I_s(\tau)I_s(t+\tau)\rangle}{\langle |I_s(\tau)|^2\rangle} = 1 + \beta|g^{(1)}(q, t)|^2, \tag{13}$$

where β is an instrumental constant between 0 and 1, called the coherence factor. The second equality in Eq. (13) is known as the Siegert relation, and is valid when $E_s(t)$ is a Gaussian random variable; under these conditions, which are usually not difficult to satisfy reasonably well, a measurement of the intensity correlation function yields direct information on S(q, t). Dynamic light scattering instruments are commercially available [34–36]. The most important component is the correlator, which forms a discrete version of $g^{(2)}(q, t)$ from the pulses emanating from a photon counting detector. Such correlators have become remarkably sophisticated and relatively inexpensive over the past decade.

The primary application of DLS is to dilute polymer solutions, where S(q, t) has the simple form:

$$S(q, t) = S(q, 0)\exp[-\Gamma t] = S(q, 0)\exp[-q^2 D_m t], \tag{14}$$

where Γ is the decay rate, and D_m is the mutual diffusion coefficient (i.e., the diffusion coefficient by which the concentration fluctuations, δc, relax). As $c \to 0$, $D_m \to D_o$, the infinite dilution translational diffusion coefficient of the polymer chains. Through the Stokes-Einstein relation,

$$D_o = \frac{kT}{6\pi\eta_s R_h}, \tag{15}$$

the particle hydrodynamic radius, R_h, can be determined; η_s is the solvent viscosity. Indeed, the principal analytical use of DLS is in particle sizing, for particles in the range 5 nm to 5 μm. Solid particles, as opposed to flexible polymer chains, can scatter intensely, and a reasonable correlation function can usually be obtained and analyzed in minutes. For a distribution of molecular weights or particle sizes, one has a corresponding distribution of decay rates, $G(\Gamma)$:

$$g^{(1)}(q, t) = \int_0^\infty G(\Gamma)\exp(-\Gamma t)\, d\Gamma, \tag{16}$$

and thus the correlation function will be a distribution of exponentials. Ideally, one would simply perform Laplace inversion on Eq. (16) to extract $G(\Gamma)$, but this is a notoriously ill-posed problem for data obtained over a finite time window, and in the presence of noise. However, a great deal of effort has been expended in this direction, and a battery of methods to analyze experimental correlation functions are now available [37–40]. The distribution of decay rates can be reliably characterized as to mean and breadth, and whether it is unimodal or bimodal; more detailed information requires extremely precise data.

Recently, there has been significant progress in extending DLS to non-dilute, and even turbid, systems. One approach, termed "diffusive wave spectroscopy" [41], takes advantage of multiple scattering of light in samples such as concentrated colloidal suspensions. In effect, each single scattering event contributes a small phase shift to the scattered wave, with the distribution of total phase shifts after multiple scattering determined by the statistics of the particle positions, and the decay of correlations determined by short-range particle motions. Another promising technique is to use a single-mode optical fiber as the receiving optics [42, 43]. In this

case, as the fiber only accepts a single mode from a potentially very complicated total scattered field, it is possible by suitable positioning of the fiber to reject all but the desired, singly-scattered, signal. One possible application of this technique is to follow polymer motions in porous media, such as packed columns.

Example 3. Systematic application of DLS to block copolymer liquids has only recently begun. As an illustration, consider the correlation function shown in Fig. 8 a [44]. It was obtained at a scattering angle of 90°, from a 10% solution of a symmetric PS-PI diblock copolymer ($M = 1.5 \times 10^5$) in toluene, a good solvent for both blocks. Although $g^{(2)}(t)$ decays smoothly to the baseline, it represents a broad distribution of decay rates; note that the time axis is logarithmic. In Fig. 8 b, the corresponding distribution of decay rates, $G(\Gamma)$, is shown; this was obtained by the Laplace inversion routine CONTIN [38]. Clearly, the spectrum is dominated by two modes, with the slower mode having significantly larger amplitude. In Fig. 8 c, the mean decay rates of the two modes are shown as a function of q^2, following Eq. (14). The fact that both data sets are linear, with zero intercept, indicates that both modes are diffusive in origin. The issue of interest is to identify the physical origin of the two modes.

In general, for a block copolymer solution one can expect two relaxation modes, because (from a scattering perspective) it is a three component system. There are thus three binary mutual diffusion coefficients, leading to two independent modes in an incompressible system. Thus, the observed decay rates correspond to the eigenvalues of a 2×2 relaxation matrix, but the identity of the eigenvectors is not known a priori. Benmouna, Akcasu and coworkers have considered this problem in detail [45, 46], but so far explicit identification of the modes is only possible under rather restrictive circumstances. A conceptually simple possibility is that one mode corresponds to relaxation of concentration fluctuations of polymer relative to solvent, a "cooperative" mode, and the other to relaxation of fluctuations of one block relative to the other, an "interdiffusion" mode. The concentration dependence and the magnitude of the decay rate of the faster mode in Fig. 8 indicates that it is, indeed, a cooperative diffusion mode [40]; it increases modestly ($D \sim c^{0.7}$) with concentration, just as observed for homopolymer solutions in the same concentration regime. The slow mode, however, appears to correspond closely to translational diffusion of the polymer chains. It decreases strongly with increasing concentration, and matches reasonable estimates for the magnitude of the translational diffusion coefficient. A similar observation has been reported previously [47]. Recent theoretical treatments suggest that this mode is, indeed, translational motion, and is visible due to compositional polydispersity, i.e., the distribution of fractional composition, f, for chains of constant N [48]. Current interest also centers on the behavior of these modes as the ODT is traversed.

Example 4. In the previous case, the solvent was good for both blocks, and thus "neutral". In a "selective" solvent, one of the blocks is preferentially solvated, and micellization can occur. DLS is an excellent technique for examining this phenomenon, because scattering in general is very sensitive to the appearance of large objects, such as aggregates, and because the temporal dimension of DLS permits resolution of the free chain mobility from that of the aggregates. There have been many studies

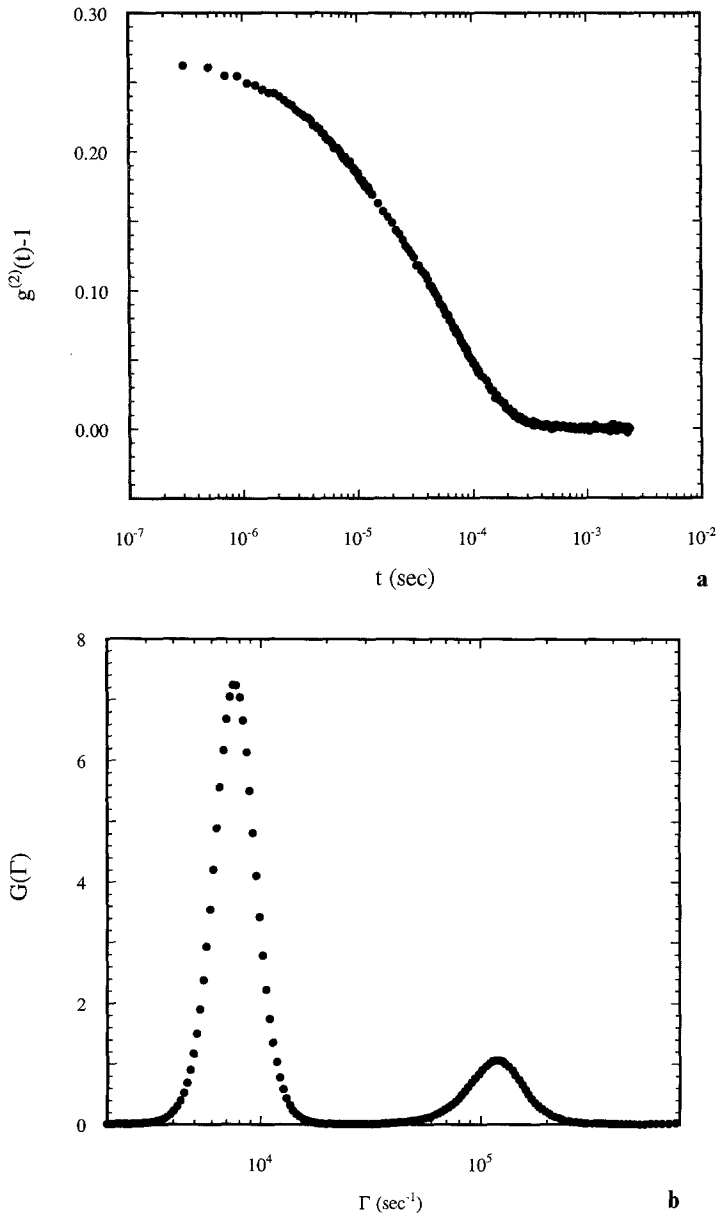

Fig. 8. Dynamic light scattering results for a 10% solution of PS-PI copolymer ($M_w = 1.4_5 \times 10^5$) in toluene [44]: **a** normalized intensity correlation function at a scattering angle of 90°; **b** Laplace inversion of the correlation function in (**a**); **c** q dependence of the two modes indicated in (**b**)

of block copolymer micellization, and the topic has been reviewed [49, 50]. In a recent example from our laboratory, Balsara examined the behavior of poly(2-vinylpyridine) (PVP)-PS-PVP symmetric triblock copolymers in toluene, a very poor solvent for PVP [51]. Diblock PS-PVP copolymers would certainly tend to micellize in toluene, but the triblock architecture offers additional possibilities. For example, there would be an additional entropic penalty if the two ends of one polymer were to lie in the central, non-dissolved core of one micelle, which might

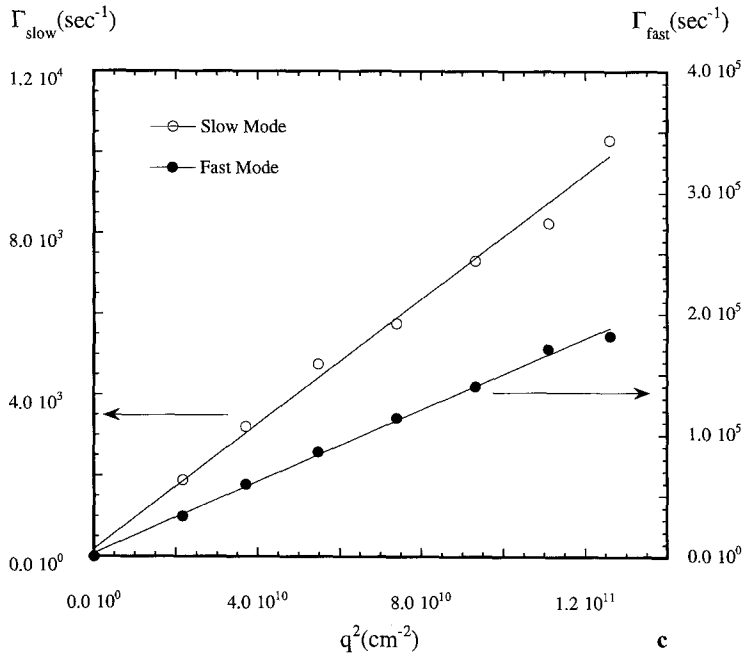

Fig. 8. (Cont.)

favor single chain dissolution, or even tenuous, three dimensional network-like aggregates. However, the DLS results demonstrated clearly that discrete micelles could form from PVP-PS-PVP chains. Figure 9 a displays the Laplace inversion of a correlation function obtained on a solution of PVP-PS-PVP chains with block molecular weights of 2.6, 2.4, and 2.6 $\times$ 10^4, respectively. The larger peak with the lower average decay rate corresponds to the micelles, whereas the smaller peak reflects the free chains. The diffusive behavior of both modes is indicated in Fig. 9 b, and thus hydrodynamic radii could be extracted via Eq. (15). The resulting values were 51 nm for the micelle, and 5.7 nm for the free chain. The latter number may be compared to the value of 7.1 nm which would be expected for a PS homopolymer of the same total molecular weight. This suggests that the free triblock copolymers adopt a smaller conformation, due to the unfavorable PVP-solvent interaction. Note also from Fig. 9 a that the distribution of micelle mobilities is relatively narrow, suggesting a single architecture for the aggregates.

C. Small-Angle Neutron Scattering (SANS)

As identified in Section II, the primary motivation for the application of SANS to polymers is the remarkable coherent contrast between ^1H and ^2H, allowing for relatively straightforward and non-intrusive labelling of organic systems. Furthermore, the typical q range allows lengthscales from 5 to 500 Å to be probed, which matches the size range of all but the largest macromolecules. SANS measurements can be performed at an increasing number of locations around the world, with the primary reactor facilities in the US being at the National Institute for Standards and Technology (NIST) and at the Oak Ridge National Laboratory (ORNL). It is

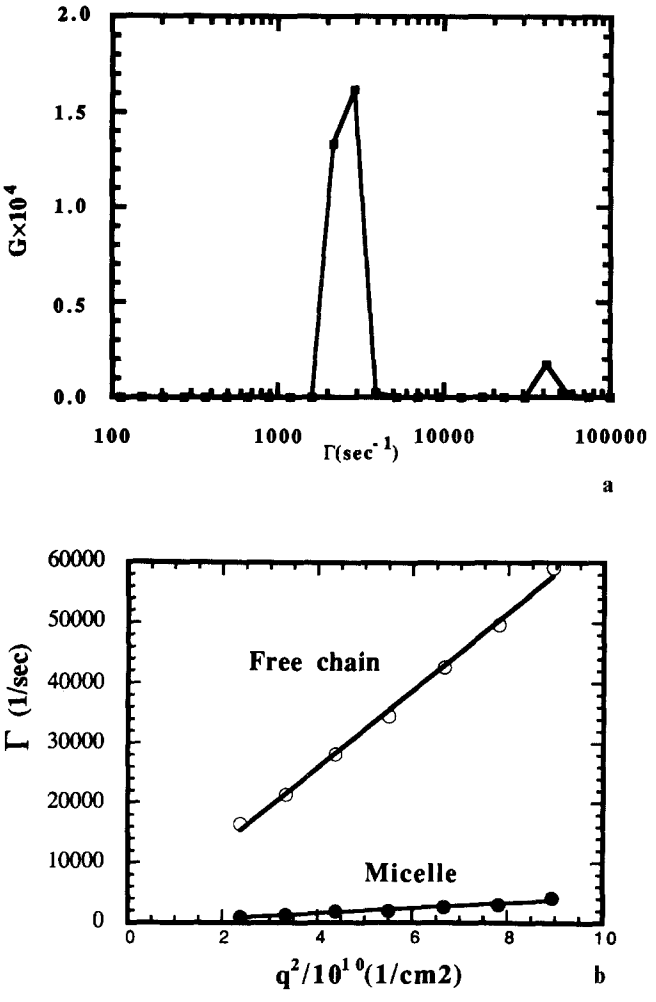

Fig. 9. Dynamic light scattering results for a PVP-PS-PVP triblock copolymer in toluene: **a** Laplace inversion of a correlation function, indicating two modes; **b** q dependence of the two modes, corresponding to diffusion of the micelles and the free chains. Reproduced, with permission, from [51]

also possible to conduct scattering experiments with neutrons from spallation sources, such as those at the Argonne and Los Alamos National Laboratories. A generic SANS spectrometer may be described as follows. Thermal neutrons emerging from a reactor in the appropriate direction enter an evacuated flight tube. In this case, thermal indicates a Maxwellian velocity distribution, with a peak energy near 0.025 eV, corresponding to $\lambda \approx 1.8$ Å. A band of wavelengths ($\Delta\lambda/\lambda \approx 0.2$) is passed by a velocity selector (e.g., a cylinder of opaque material with a helical slot, that rotates around the long axis at a selected rate), and is incident on the sample after passing through two or more apertures to define $\mathbf{k}_i$. For polymer samples, λ varies between 4 and 10 Å, which would mean a severely reduced flux relative to the peak of the distribution. In order to increase the flux, a "cold source" is used, in which the thermal neutrons are further slowed by multiple collisions with liquid H_2. The sample is typically 1 cm × 1 cm, corresponding to the cross section of the incident beam, and between 0.1 and 1 cm thick, depending on the amount of incoherent scattering and/or absorption. Scattered neutrons are collected by an area detector, which is 1 m × 1 m with either 64 × 64 or 128 × 128 pixels, placed between 3 and 30 m away from the sample. Clearly, moving the detector away from

the sample increases the resolution but decreases the signal; the standard placement would yield the minimum necessary resolution for a given experiment. This is directly analogous to dispersive spectroscopy in the weak signal limit, with slit widths adjusted to give the minimum acceptable resolution. The neutron flux at the sample is on the order of 10^6–10^8 neutrons/s, which is ten orders of magnitude or more below the photon flux from a typical laser. Three recent applications to block copolymers will serve to illustrate the kind of chain conformation and supramolecular structural information that SANS can provide.

Example 5. As illustrated in Fig. 3 and discussed in Section III, the individual chains in a strongly ordered block copolymer have end-to-end vectors normal to the interface, on average, and are stretched along the normal. There have been several experimental attempts to quantify this effect [49, 52–54], by mixing labelled and unlabelled diblock copolymers, i.e., hA-B and dA-B, where the h and d prefixes denote protonated and deuterated materials, respectively. The experiment is more complicated than a straightforward determination of chain dimensions in the bulk, however. First, it is necessary to introduce macroscopic order into the samples by aligning the lamellae, or the presumed anisotropy of the block conformations will be averaged out. This can be achieved by careful solvent casting, or by the application of shear flow. Second, unless the scattering contrast per unit volume is closely matched between the A and B microdomains, there will be substantial scattering from the lamellar pattern itself. This can be sufficiently strong to prevent accurate determination of $R_{g,z}$, the component of R_g normal to the interface. In the most recent studies of this type, PS-PVP copolymers were used [53, 54]; the scattering power of PVP is intermediate between hPS and dPS. Thus, by blending the h- and d-labelled copolymers in the appropriate ratio, the average contrast of the two microdomains should be equivalent. (Note that in SANS it is not necessary to use a dilute amount of the labelled species in order to determine R_g, if the single chain form factors of the h- and d-chains are otherwise identical; this "high-concentration" labelling scheme has proven to be very powerful in examining conformations in bulk polymers [6]). Even in this optimum case, however, it proved difficult to extract $R_{g,z}$ precisely. However, consistent with the previous results [52], it was found that $R_{g,x}$ ($=R_{g,y}$) was about 70% of the unperturbed value, while $R_{g,z}$ was expanded by a comparable factor [53]. In a further study, the labelling was confined to a portion of the PS block, either at the free end or adjacent to the junction point [54]; the samples were thus triblock copolymers of dPS-hPS-PVP and hPS-dPS-PVP. In this way it was possible to show that the segments near the chain junction were located near the interfacial regions, and anisotropic in conformation, whereas the segments near the free ends were located in the middle of the microdomains, and isotropic; this is completely consistent with the physical picture illustrated in Fig. 3.

Example 6. As mentioned in Section III, there is experimental evidence that stretching of the individual block copolymer chains begins in the fluctuation regime, i.e., in the disordered state but close to the ODT [21]. This conclusion is based on SANS measurements of a series of partially deuterated, symmetric PEP-poly(ethylethylene) (PEE) samples. The degree of polymerization, N, was varied from 125 to 1890, such that the ODT at room temperature corresponded to $N \approx 800$. For all the samples,

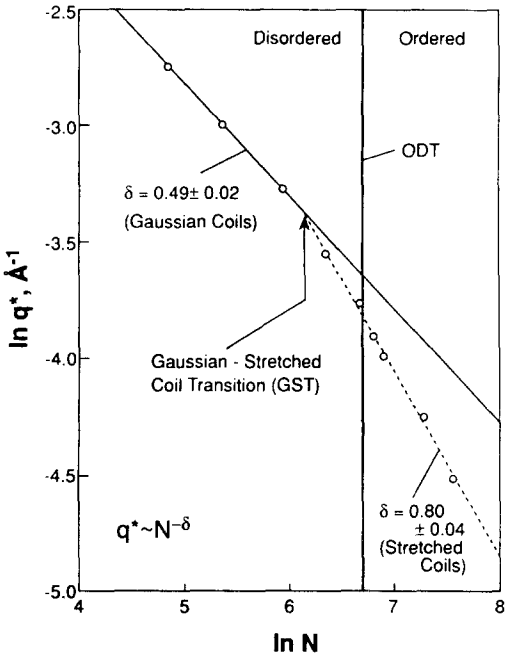

Fig. 10. Variation of the position of the maximum in scattered intensity with chain degree of polymerization, indicating the stretching of the copolymer chains prior to the ODT. Reproduced, with permission, from [21]

the measured intensity exhibited a peak at a finite value of q, designated q*. For the ordered samples, the origin of this peak is clear: it reflects the lamellar period. In the disordered state, however, it is also an expected feature: the chain architecture leads to a preferred intermolecular distance between two similar blocks. The centers of mass of two "A" blocks are inhibited from approaching closely by the presence of the attached "B" blocks. In both cases, $2\pi/q^*$ corresponds to a molecular length-scale on the order of R_g. In Fig. 10, q* is plotted against N in a double logarithmic format. At low N, in the disordered state, $q^* \sim N^{-0.5}$, as expected for Gaussian coils, but above a certain N, $q^* \sim N^{-0.8}$, corresponding to stretched coils. Interestingly, this latter exponent is greater than the 0.67 expected well into the ordered state. This is a crossover effect, which has been partly quantified in more recent calculations [55]. The physical origin of the early onset of stretching was alluded to in Section III. If one imagined cleaving a symmetric block copolymer of total length N into its constituent homopolymers, they would phase separate macroscopically if $\chi N > 4$. Thus, in the regime $4 < \chi N < 10.5$, the individual blocks are, in a qualitative sense, frustrated; one way to accommodate this is for the centers of mass of two attached blocks to separate slightly, without otherwise distorting the chain conformations.

Example 7. SANS provides an excellent, non-destructive means to establish the morphology of a block copolymer in the ordered state. In this instance, SANS is complementary to electron microscopy; although microscopy provides a real-space image, it has non-trivial sample preparation requirements, and for some systems contrast may not be obtainable even by staining. Bates and coworkers have developed an extensive series of fully saturated hydrocarbon block copolymers, which fall into this class [17, 20, 21]. By catalytically hydrogenating or deuterating anionically-polymerized diene precursors, saturated materials with very narrow molecular weight and composition distributions have been prepared. One example is

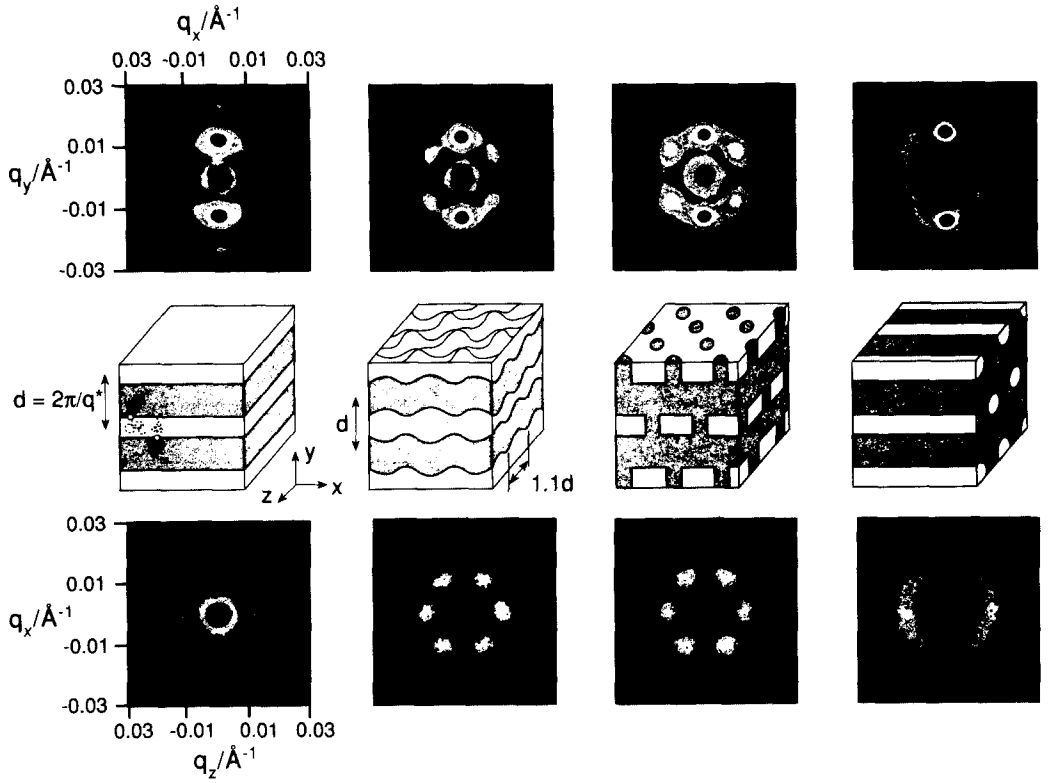

Fig. 11. Multiple ordered phases in a sheared PEP-PEE melt, f = 0.65, as a function of (increasing) temperature. The upper series of SANS intensity profiles are logarithmic, whereas the lower series are linear, to emphasize the weaker scattering peaks. The shear direction is x. Reproduced, with permission, from [57]

the PEP-PEE system, derived from poly(1,4-isoprene)-poly(1,2-butadiene), and employed in the previous example. As the resulting blocks are essentially structural isomers, the χ parameter is typically small, and large molecular weights (5×10^4–1×10^5) are required to access the ODT. This is in contrast to more extensively studied systems such as PS-PI, which is in the ordered state for all but modest molecular weights ($\leq 10^4$).

Studies with PEP-PEE and related systems have revealed unexpected richness in copolymer behavior. For example, asymmetric PEP-PEE samples (i.e., $f \neq 0.5$) have displayed a series of order-order transitions, in some cases between morphologies that were never observed previously for copolymers [56, 57]. The various states were accessed simply by varying temperature (i.e., χ) for melt samples. An example is shown in Fig. 11, showing the evolution of the scattering patterns with increasing temperature, and the corresponding proposed morphologies [57]. An important aspect of these studies is the use of large-amplitude shear flows, to produce macroscopically-aligned samples. This makes structural evaluation much more direct, just as X-ray diffraction from single crystals is more easily interpreted than the corresponding "powder pattern". Recently, a shearing device has been

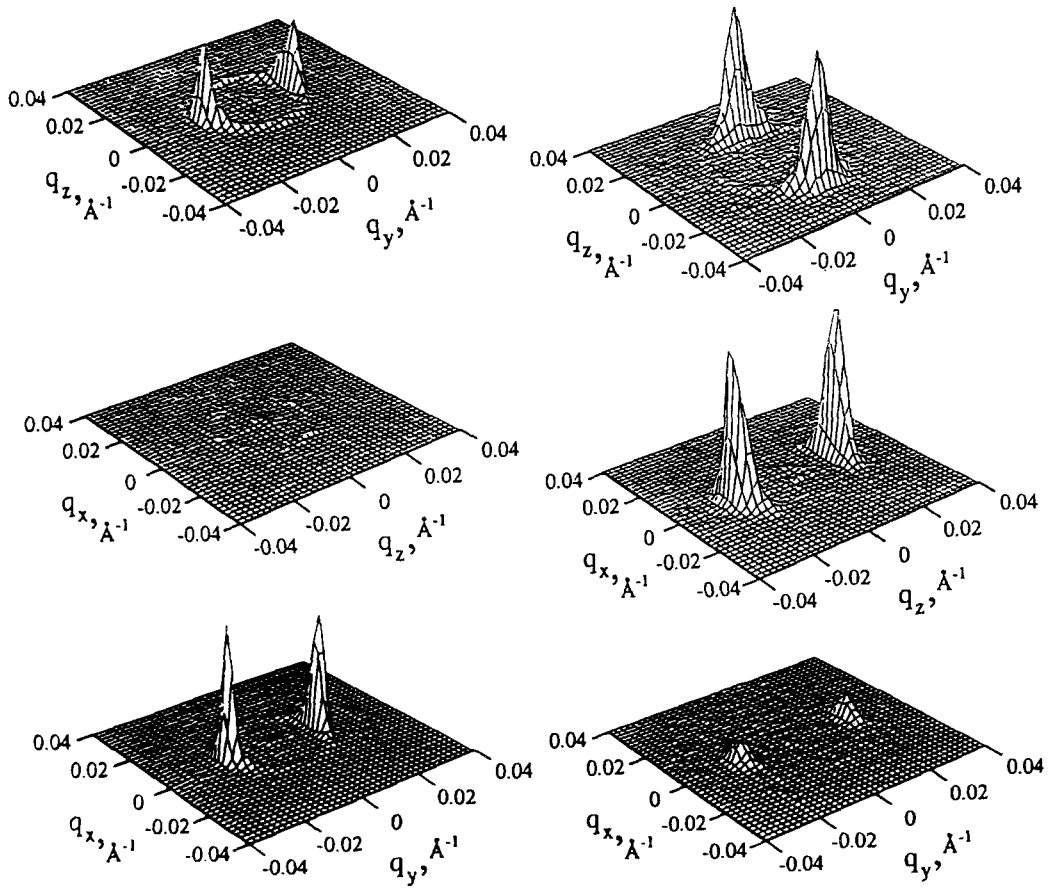

Fig. 12. SANS intensity contour plots for a symmetric PEP-PEE sample, after shearing with 100% strain amplitude for 15 hours. The shear direction is x, and the gradient direction y. The sample on the left was sheared at 0.02 rad/s, resulting in "parallel" lamellae, whereas that on the right was sheared at 1.0 rad/s, leading to "perpendicular" lamellae. Reproduced, with permission, from [59]

developed that can be used directly on the SANS spectrometer, to follow the evolution of morphology in real time [58]. Interestingly, the effect of shear on a given morphology is not necessarily trivial. For example, simply by changing the frequency of the shear, it was possible to macroscopically orient a lamellar sample with the lamellar planes either parallel or perpendicular to the shear planes; the SANS evidence is shown in Fig. 12 [59]. The underlying mechanism(s) that govern the alignment process is currently an area of active research.

D. Small-Angle X-ray Scattering (SAXS)

In many respects, SAXS should be the most familiar scattering technique to chemists, bearing as it does such a close relation to X-ray crystallography. For amorphous organic materials, however, the relatively low X-ray contrast obtained makes SANS preferable, even given the much lower fluxes obtainable in neutron experiments. Therefore the major applications of SAXS to amorphous polymers have involved microstructured materials, such as block copolymers.

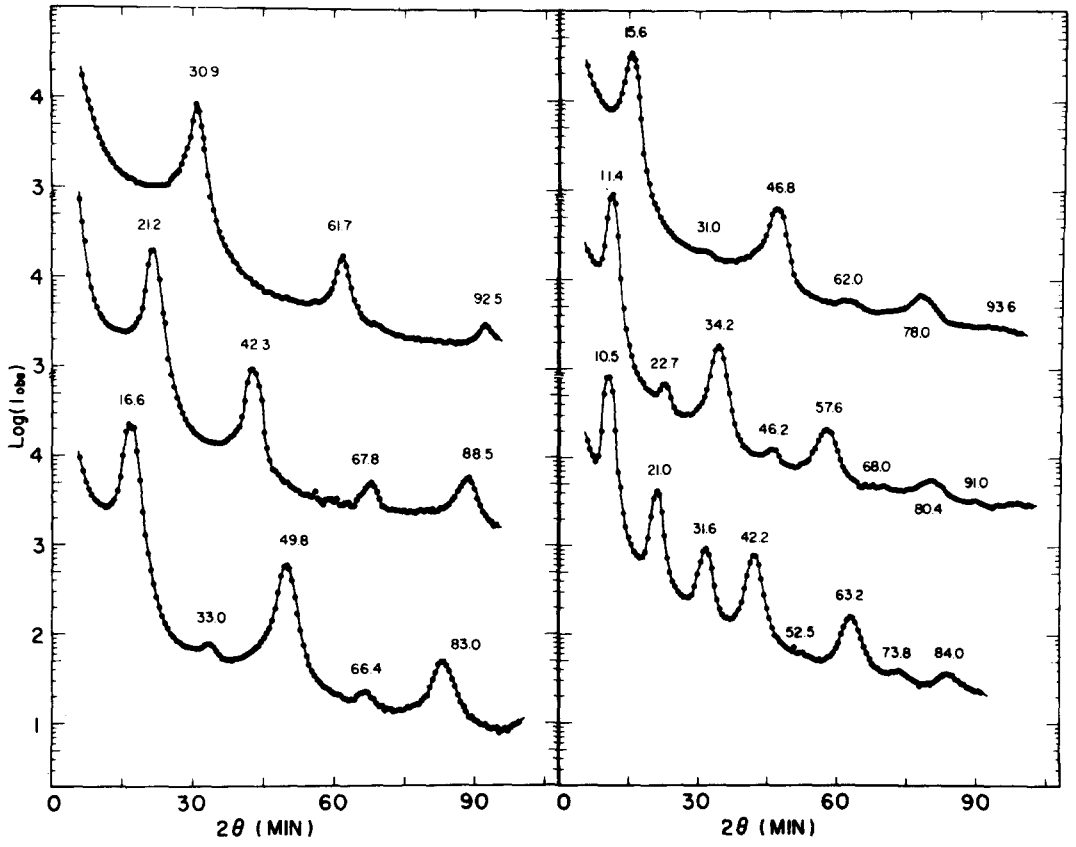

Fig. 13. SAXS intensity profiles for symmetric PS-PI diblocks of varying total molecular weight. Reproduced, with permission, from [60]

Example 8. In their pioneering studies of styrene-diene copolymers, Hashimoto and Kawai and coworkers used SAXS extensively to explore the various morphologies, and to investigate particular issues such as the molecular weight dependence of the domain spacing, and the interfacial width [60]. In Fig. 13, the SAXS profiles are shown for six nearly symmetric PS-PI specimens. The samples were prepared by solvent casting, followed by slow evaporation of the solvent. This results in highly oriented lamellar microdomains, and the results in Fig. 13 correspond to the incident beam propagating parallel to the lamellar planes. The peaks confirm the lamellar morphology, because they occur at integer multiples of the primary peak position (q_{max}). The relative heights of the various maxima depend primarily on the volume fractions of the two components, whereas the number of maxima that are visible depends on the degree of macroscopic orientation and the constancy of the domain spacing. The resulting average domain spacings are plotted as a function of molecular weight (double logarithmically) in Fig. 14; the slope of 2/3 is in excellent agreement with the strong segregation prediction. Also shown in the figure are estimates of the width of the interfaces between the PS and PI domains. These were obtained from analysis of the scattering at higher angles than shown in Fig. 13. As expected, the interfacial width is independent of molecular weight, but forms a substantial part of the lamellar period for low molecular weight chains.

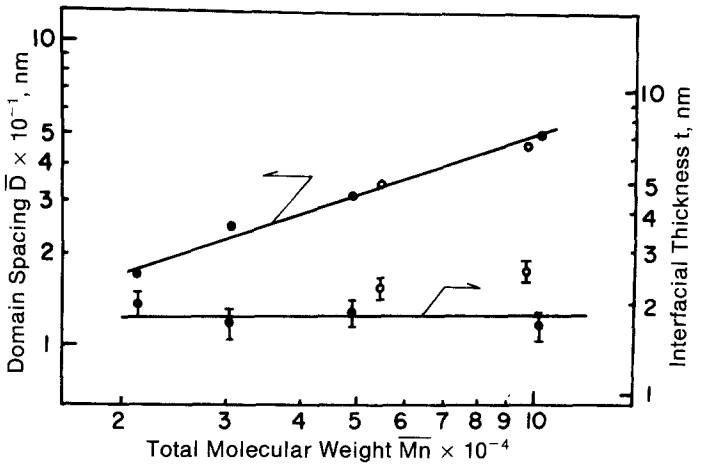

Fig. 14. Domain spacing and interfacial thickness as functions of molecular weight for the PS-PI lamellae of Fig. 13. Reproduced, with permission, from [60]

Example 9. The advent of synchrotron sources for X-ray scattering opens up further possibilities, because of the greatly increased flux over typical laboratory scale instruments. For example, it is now possible to examine the time evolution of block copolymer microstructures with temporal resolution below one second. Singh et al. recently reported an experimental study of the response of styrene-butadiene solutions to a temperature quench from the disordered into the ordered regime [61]. One expects, in such a case, to observe at least two processes: the rapid ordering, or microphase separation, of chains at the local scale, followed by a slower growth of longer-range order, or "grains". In this particular study, only the latter stage was clearly resolved. Interestingly, the time dependence revealed two regimes: a constant nucleation rate at early times, followed by later time behavior suggestive of heterogeneous nucleation on two-dimensional defect sites. This kind of nucleation and growth process has been described by Cahn [62], and a scaled plot of the data for several samples and quench experiments, following Cahn's analysis, is shown in Fig. 15. The limiting slopes of $+4$ and $+1$ correspond to the two processes identified above, and the success of the superposition is reasonable. The origin of the apparent two-dimensional defect sites is not obvious, however, given that the systems adopted the spherical (bcc) morphology. Nevertheless, this work demonstrates both the feasability of the technique and the richness of the phenomenology.

E. Neutron Reflection (NR)

Neutron reflection is a relatively new technique to polymer science, and provides a unique means to characterize the atomic composition as a function of depth in a thin film. Technically, NR and X-ray reflection are not scattering experiments, per se, but the similarities with the corresponding small-angle scattering experiments are so extensive that it is completely appropriate to consider them together. As with SANS, the contrast between ^1H and ^2H is the key to the utility of NR, and the characteristically short wavelengths give depth resolution on the Ångstrom scale. The basic experiment is illustrated in Fig. 16. A beam of neutrons strikes the sample

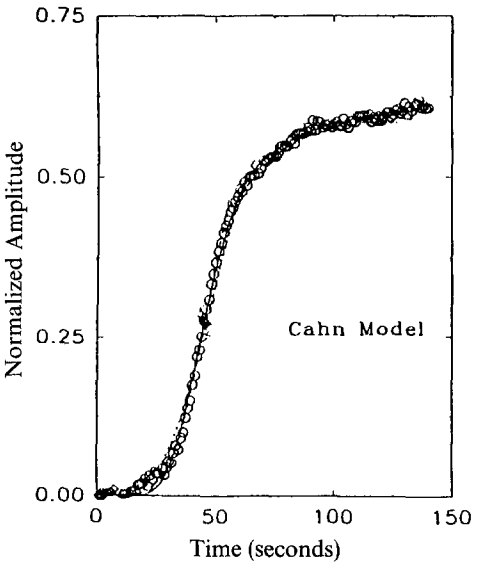

Fig. 15. Time evolution of the peak x-ray scattering intensity following a temperature quench into the ordered state, for a PS-PB copolymer solution. Adapted, with permission, from [61]. $T_i = 159.6°C$, $T_f = 94.0°C$

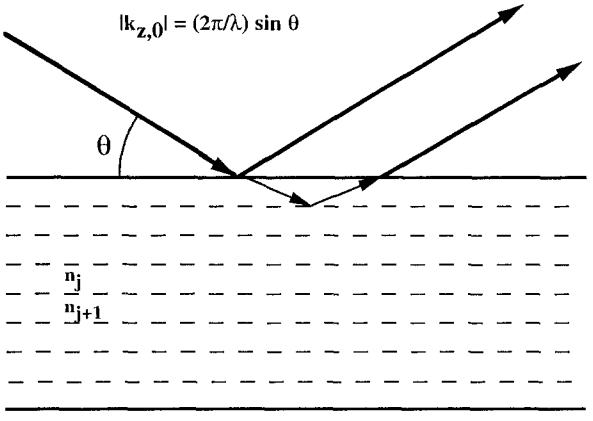

Fig. 16. Schematic illustration of the neutron reflection experiment

at near-grazing incidence, and the specularly-reflected beam intensity is detected. The film can be pictured as a series of thin layers, each with characteristic refractive index n(z), where z is the depth. The reflected beam will be the superposition of waves reflected from each layer, analogous to optical reflection from multilayer coatings. The reflectivity profile, $R(k_z)$, is thus related to the composition profile through n(z); k_z, the z component of the wavevector, can be varied by changing λ or the angles of incidence and reflection.

For neutrons in non-magnetic media the refractive index can be written [8, 9]

$$n = 1 - \delta + i\beta, \tag{17}$$

where

$$\delta(z) = \frac{\lambda^2}{2\pi} \sum_j N_j(z) b_j, \tag{18}$$

with N_j and b_j the number density and coherent scattering length for atom j. The parameter β characterizes absorption, which can usually be neglected for organic

systems. Typical values of δ are on the order of 10^{-6}, and thus n is only slightly less than 1. Application of Snell's law provides the critical angle for total external reflection, θ_c, as

$$\theta_c = \sqrt{2\delta}, \tag{19}$$

at the air interface. Note that it is customary in NR to define the angle θ between the incident beam and the surface, rather than relative to the normal as in traditional optics. For specular reflection, one is only concerned with k_z, and the reflection coefficient at the interface between layers j and j + 1 is given by the Fresnel equation

$$r_{j,j+1} = \frac{(k_{z,j} - k_{z,j+1})}{(k_{z,j} + k_{z,j+1})}. \tag{20}$$

The leads to a measured reflectivity, $R(k_z)_{j,j+1}$ given by

$$R(k_z)_{j,j+1} = r_{j,j+1} r^*_{j,j+1}. \tag{21}$$

For the macroscopic film, the measured reflectivity involves the superposition of terms as in Eq. (21) from each interface; each $k_z(z)$ depends on n(z), and the phase factor in the superposition depends on the thickness of each layer. For a continuous distribution,

$$\begin{aligned} R(k_z) &\propto \left| \frac{1}{k_z} \int_{-\infty}^{\infty} n(z) e^{ik_z z}\, dz \right|^2 \\ &\propto \left| \frac{1}{k_z^2} \int_{-\infty}^{\infty} \frac{\partial n}{\partial z} e^{ik_z z}\, dz \right|^2. \end{aligned} \tag{22}$$

The interpretation of a measured reflectivity profile requires some care. As the signal contains only amplitude information, direct Fourier inversion is not usually feasible. A standard approach, therefore, is to guess a plausible form for n(z), either in continuous or discrete form, and to fit the data by adjusting the parameters. This can be extremely tedious when there are several parameters involved, and one can never prove the uniqueness of the resulting composition profile. However, the recent increase in applications of reflectivity techniques to polymer systems has inspired some efforts to devise more general approaches [8, 11].

Example 10. It is well-established that surfaces can induce order in polymer mixtures, due to differences in the surface energetics of the components. For lamellar PS-PMMA block copolymers on silicon, for example, the PMMA block preferentially wets the silicon surface whereas PS predominates at the air interface [63]. If the sample is below the bulk ODT, therefore, the surface can induce a macroscopic alignment of the lamellae parallel to the surface, if the sample is annealed for a sufficient length of time above the glass transition temperature of both blocks. This is illustrated in Fig. 17. A film of a PS-PMMA copolymer was cast on a fused silica substrate, and the reflectivity profile shown in Fig. 17 a obtained. Note that below a certain k, total external reflection occurs, whereas with increasing k, the reflectivity drops by a factor of 10^5. This wide dynamic range is typical of NR; in X-ray reflectivity, much greater ranges can be obtained, due to the higher incident flux [8]. The slight dip in reflectivity at very low k is due, at least in part, to shadowing: the area illuminated by the incident beam is larger than the sample. The high frequency

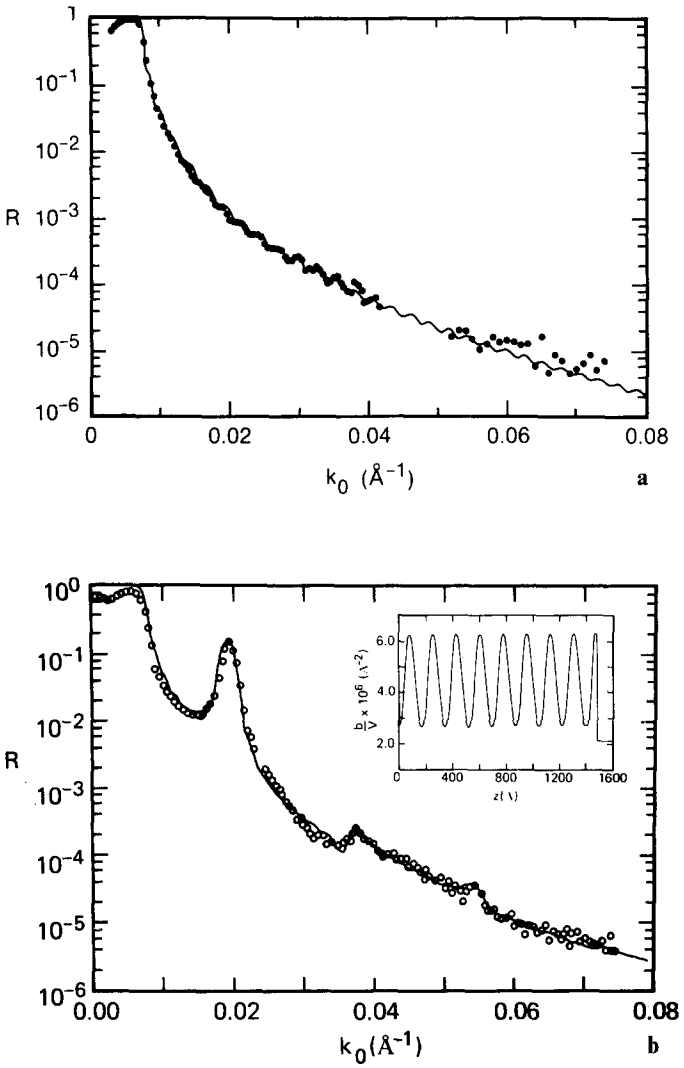

Fig. 17. Neutron reflectivity profiles for a PS-PMMA film on silicon, **a** as cast, and **b** after annealing. Reproduced, with permission, from [63]

oscillations in the reflectivity profile are the so-called "Kiessig fringes", resulting from interference between reflections from the top and bottom surface of the film. The smooth curve through the data is a fit using a film of constant scattering length density and a thickness of 1140 Å. Subsequently, the sample was annealed above the glass transition temperatures of the components, but below the ODT. The preferential wetting of the silicon interface by the PMMA, and the air interface by the PS, induces a complete orientation of the lamellae parallel to the substrate surface. The data are fit by the reflectivity profile shown in the inset.

In Fig. 18, the reflectivity profile is shown for another PS-PMMA copolymer film on silicon, after annealing. In this case, the total film thickness corresponded to a monolayer of copolymer, such that after annealing, a single lamella was formed. The data were fit with a hyperbolic tangent function to describe the PS-PMMA interface, with the interfacial width fixed at 50 ± 5 Å. It is important to note that the scattering length densities are well-known for the various components, so the amplitudes of the profiles used to simulate the data are not freely adjustable. The

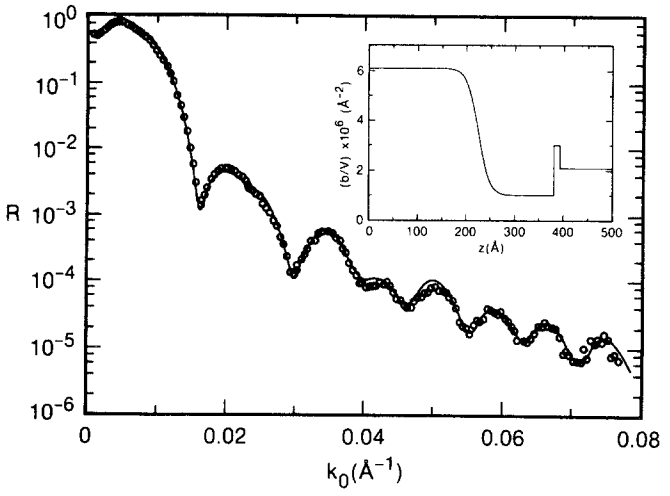

Fig. 18. Neutron reflectivity profile for a PS-PMMA film on silicon; composition profile used to fit the data shown in the inset. Reproduced, with permission, from [63]

small spike at the silicon/PMMA interface is attributed to the formation of a 10 Å oxide layer.

Example 11. Even above the bulk ODT, the preferential wetting of the surface can induce structure that extends for a significant distance into the film (i.e., beyond one lamellar period). Foster et al. have reported a detailed NR study of nearly symmetric PEP-PEE block copolymer thin films on silicon wafers [64]. A series of molecular weights were employed, such that the samples ranged from well above to well below the ODT at room temperature, in the bulk. The reflectivity data for six samples are shown in Fig. 19 a, along with the fitted concentration profiles. The peak heights from these various samples can not be compared directly, as each sample has a different degree of ^1H and ^2H substitution. The high frequency oscillations in the lowest M sample are the Kiessig fringes; the other samples were sufficiently thick that these fringes are not resolved.

The PEE composition profiles used to fit the data are shown in Figure 19 b; several interesting features emerge. First, as M increases, the degree of segregation increases, and the interfacial profiles sharpen. For the highest M sample, the volume fraction of PEE is either 1 or 0 for a significant fraction of the film, suggesting that the sample is in the strong-segregation limit. However, the interfacial width of 63 ± 3 Å is still considerably broader than the predicted limiting value of 40 Å. For the lowest M, the sample appears to be completely disordered, except for a thin layer of PEE that wets each surface. However, this observation is also noteworthy. If the surface enrichment were enthalpy-driven, as it is in PS-PMMA and most polymer blends, different components would wet the two surfaces. In the PEP-PEE case, the enthalpic part of the surface interaction must be very similar for the two blocks, as they are both simple alkanes. Therefore, it appears that the segregation is entropy-driven. PEE has a smaller statistical segment length, meaning that it is easier for this polymer to accommodate packing near a flat surface. This interpretation has some theoretical support [65].

In the bulk at room temperature, the N = 791 sample would be just in the disordered state ($T_{odt} \approx 16°C$), but in Fig. 19 b considerable order is still apparent throughout the film. As discussed in Section III, there is extensive evidence for

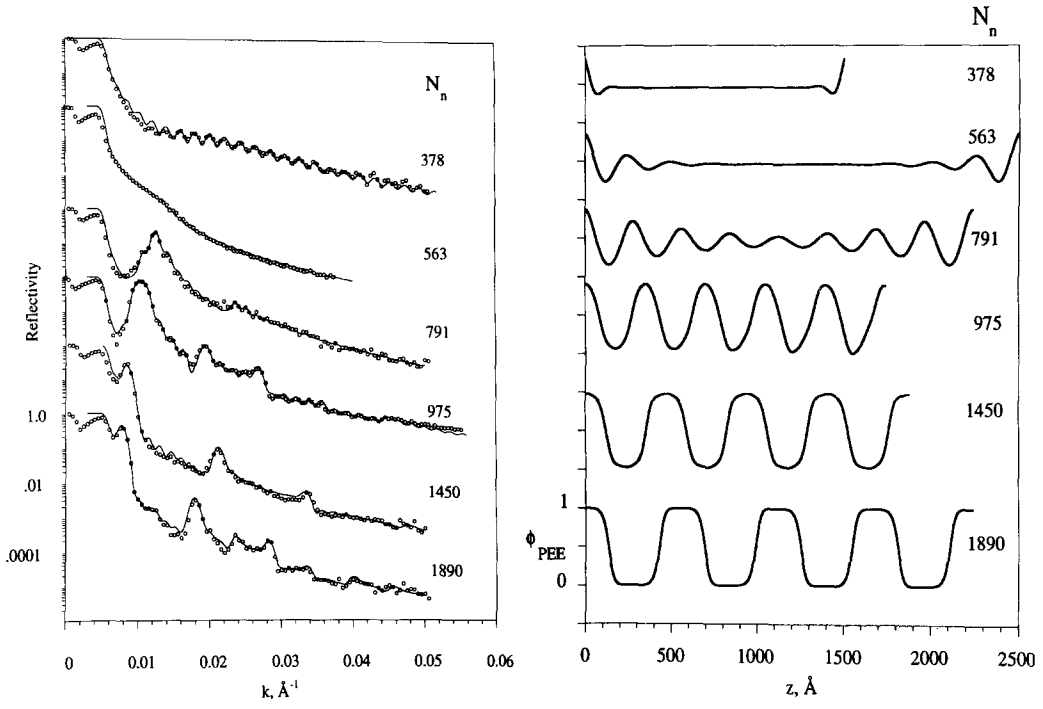

Fig. 19. Neutron reflectivity profiles and corresponding concentration profiles for a series of PEP-PEE films on silicon. Reproduced, with permission, from [64]

substantial composition fluctuations in bulk samples above the ODT. These results could be interpreted, therefore, as a surface-induced coherence to these fluctuations, with a correlation length of several hundred Å. It is important to emphasize, however, that NR is only sensitive to the z component of the composition profile. The center of this film, which appears to be uniform in composition by NR, could actually exhibit composition profiles with the same magnitude as at the edges, only with random orientations.

F. X-ray Reflection (XR)

X-ray reflection bears much the same relation to NR as SAXS to SANS. On the one hand XR instruments exhibit much higher incident fluxes, but polymer-polymer contrast is harder to achieve. In addition, it should be noted that the much higher photon energy in the X-ray case raises some possibility of sample degradation. Nevertheless, XR is proving to be very useful for characterizing thin polymer films. The particular strength of XR is in examining total film thickness, and the relative smoothness of the air-polymer and polymer-substrate interfaces. This is because the change in electron density is generally quite large at the boundaries of the film. NR, in contrast, is particularly suited to the characterization of internal, or "buried" interfaces, when appropriate isotopic substitution is used.

Example 12. In examples 10 and 11, thin block copolymer films developed lamellar order with a constant number of layers. If one casts an intermediate amount of

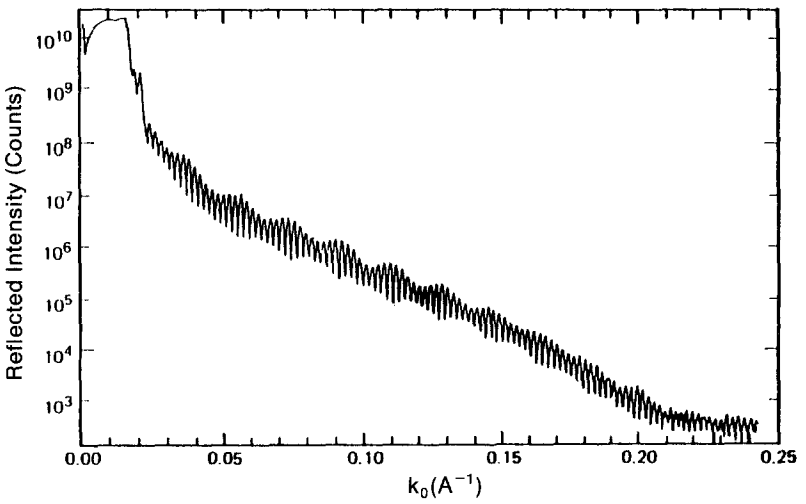

Fig. 20. X-ray reflectivity profile from a PS-PMMA diblock copolymer film, which has "islands" exactly one lamella thickness high, on the air surface. Reproduced, with permission, from [8]

material onto a substrate, the sample has to choose whether to have n or n + 1 layers; this results in "islands" or "holes" on the surface, because the total thickness is quantized. An example is shown in Fig. 20, for a PS-PMMA diblock (for this system, with PMMA at the substrate surface and PS at the air surface, the system must choose between n ± 1/2 layers) [8]. The presence of two layer thicknesses results in beating between two frequencies, clearly visible in the figure; the higher frequency oscillations correspond to the average film thickness.

V. Summary

In this review we have attempted to describe the basic features of scattering experiments, and to summarize salient aspects of each of six techniques of current importance in polymer characterization. Selected examples of recent applications have been provided, to illustrate the quality of the information that can be obtained. Most of these applications highlight block copolymer systems, which constitute one of the most vigorous areas of contemporary research in polymer science and technology. The major points that have been underscored in this review are as follows:

- Scattering arises from *fluctuations* in a material; usually it is spontaneous concentration fluctuations that are of interest. The dependence of the scattered intensity on scattering angle, or q, reflects the spatial arrangement or *structure* of the sample.
- The scattered intensity always depends on the *contrast*; the skillful manipulation of contrast permits extremely detailed examination of structure in polymer solutions, melts, and solids.
- The *lengthscales* of interest, $2\pi/q$, range from 10 to at least 10^4 Å, and are thus complementary to optical microscopy. Furthermore, this range matches exactly the relevant dimensions in polymer systems.
- Scattering techniques provide a *Fourier space image* of the structure. Consequently, there is often an inversion problem that can not be solved uniquely in the

general case. However, in some instances, unambiguous information can be obtained, such as the molecular weight and the radius of gyration. Furthermore, in most other cases there is sufficient information available a priori that the data may be interpreted reliably.

– The scattering process is usually *statistical*, arising from fluctuations in equilibrium systems. Consequently, signal-to-noise ratios are not high, relative to many other analytical techniques, and substantial averaging times may be required. However, advances in instrumentation, combined with judicious choice of labelling schemes, serve to ameliorate this situation.

– Light scattering is the most commonly applied scattering technique for polymer systems. Powerful static and dynamic light scattering instruments are commercially available, and the high photon flux from laser sources helps to mitigate the signal-to-noise issue. Most applications are to dilute solutions, and the largest experimental hurdle is the preparation of sufficiently dust-free samples.

– Neutron scattering suffers from characteristically low incident fluxes, and can only be performed at a handful of sites around the world. However, the remarkable contrast between ^{1}H and ^{2}H makes the neutron techniques unique in their ability to investigate structural details in organic materials.

– X-ray scattering is intermediate between light and neutron scattering in terms of available flux. The accessible lengthscales are comparable with neutron scattering, but it is harder to obtain contrast at the molecular scale in amorphous hydrocarbon polymers, so most applications emphasize microstructured materials, which have characteristically large concentration fluctuations.

– Reflectivity techniques are relative newcomers to polymer characterization, but have tremendous potential to probe the structure of thin films, with Ångstrom resolution.

Acknowledgement. The financial support of the National Science Foundation, through grant DMR-9018807, and the University of Minnesota Center for Interfacial Engineering, an NSF-supported Engineering Research Center, is gratefully acknowledged.

References

[1] M. B. Huglin (ed.), *Light Scattering from Polymer Solutions*, Academic Press, New York, 1972.
[2] P. J. Wyatt, *Anal. Chim. Acta* **1993**, *272*, 1.
[3] B. J. Berne, R. Pecora, *Dynamic Light Scattering*, Wiley, New York, 1976.
[4] B. Chu, *Laser Light Scattering*, 2nd Ed., Academic Press, San Diego, 1991.
[5] K. S. Schmitz, *Dynamic Light Scattering by Macromolecules*, Academic Press, San Diego, 1990.
[6] G. D. Wignall (ed.), *The Encyclopedia of Polymer Science and Technology, Vol. 10*, Wiley, New York, 1987.
[7] W. Marshall, S. W. Lovesey, *Theory of Thermal Neutron Scattering*, Clarendon Press, Oxford, 1971.
[8] T. P. Russell, *Materials Science Reports* **1990**, *5*, 171.
[9] J. Penfold, R. K. Thomas, *J. Phys. Condens. Matter* **1990**, *2*, 1369.
[10] O. Glatter, O. Kratky, *Small Angle X-ray Scattering*, Academic Press, London, 1982.
[11] M. D. Foster, *Crit. Rev. Anal. Chem.* **1993**, *24*, 179.
[12] B. H. Zimm, *J. Chem. Phys.* **1948**, *16*, 1093.

[13] P. G. de Gennes, *Scaling Concepts in Polymer Physics*, Cornell University Press, Ithaca, 1979.
[14] D. J. Meier (ed.), *Block Copolymers: Science and Technology*, MMI Press/Harwood Academic, New York, 1983.
[15] F. S. Bates, G. H. Fredrickson, *Ann. Rev. Phys. Chem.* **1990**, *41*, 525.
[16] F. S. Bates, *Science* **1991**, *251*, 898.
[17] F. S. Bates, M. F. Schulz, J. H. Rosedale, K. Almdal, *Macromolecules* **1992**, *25*, 5547.
[18] L. Leibler, *Macromolecules* **1980**, *13*, 1602.
[19] G. H. Fredrickson, E. Helfand, *J. Chem. Phys.* **1987**, *87*, 697.
[20] F. S. Bates, J. H. Rosedale, G. H. Fredrickson, *J. Chem. Phys.* **1990**, *92*, 6255.
[21] K. Almdal, J. H. Rosedale, F. S. Bates, G. D. Wignall, G. H. Fredrickson, *Phys. Rev. Lett.* **1990**, *65*, 1112.
[22] B. H. Zimm, *J. Chem. Phys.* **1948**, *16*, 1099.
[23] P. Debye, *J. Appl. Phys.* **1944**, *15*, 338.
[24] M. S. Kent, *Ph.D. Thesis*, University of Minnesota, 1990.
[25] Milton Roy Company, Rochester, NY 14625.
[26] Wyatt Technology Corporation, Santa Barbara, CA 93103 .
[27] W. Yunan, X. Zhongde, J. Li, W. M. Rosenblum, J. W. Mays, *J. Appl. Polym. Sci.* **1993**, *49*, 967; S. H. Kim, P. M. Cotts, *J. Appl. Polym. Sci.* **1991**, *42*, 217.; L. Jeng, S. T. Balke, T. H. Mourey, L. Wheeler, P. Romeo, *J. Appl. Polym. Sci.* **1993**, *49*, 1359.
[28] see, for example, T. P. Lodge, P. Markland, L. M. Wheeler, *Macromolecules* **1989**, *22*, 3409; M. S. Kent, M. Tirrell, T. P. Lodge, *Macromolecules* **1992**, *25*, 5383 (and references therein).
[29] T. Tanaka, M. Omoto, H. Inagaki, *Macromolecules* **1979**, *12*, 147.
[30] M. S. Kent, M. Tirrell, T. P. Lodge, *Polymer* **1991**, *32*, 315.
[31] M. S. Kent, M. Tirrell, T. P. Lodge, *J. Polym. Sci., Polym. Phys. Ed.* **1994**, *32*.
[32] T. Sato, C. C. Han, *J. Chem. Phys.* **1988**, *88*, 2057.
[33] A. Cumming, P. Wiltzius, F. S. Bates, J. H. Rosedale, *Phys. Rev. A* **1992**, *45*, 885; A. Cumming, P. Wiltzius, F. S. Bates, *Phys. Rev. Lett.* **1990**, *65*, 863.
[34] Brookhaven Instruments Corporation, Holtsville, NY 11742.
[35] ALV-Laser Vertriebsgesellschaft mbH, D-6070 Langen, Germany.
[36] Malvern Instruments, Ltd., Malvern, Worcs., WR14 1AT, UK.
[37] D. E. Koppel, *J. Chem. Phys.* **1972**, *57*, 4814.
[38] S. W. Provencher, *Comput. Phys. Commun.* **1982**, *27*, 229.
[39] D. Sun, Z. Wang, G. Wu, B. Chu, *Macromolecules* **1992**, *25*, 1114.
[40] R. S. Stock, W. H. Ray, *J. Polym. Sci., Polym. Phys. Ed.* **1985**, *23*, 1393.
[41] D. J. Pine, D. A. Weitz, P. M. Chaikin, E. Herbolzheimer, *Phys. Rev. Lett.* **1988**, *60*, 1134.
[42] R. Brown, *Appl. Opt.* **1987**, *26*, 4846.
[43] J. Ricka, *Appl. Opt.* **1993**, *32*, 2860.
[44] C. Pan, W. Maurer, Z. Liu, T. P. Lodge, P. Stepanek, E. D. von Meerwall, H. Watanabe, *Macromolecules* (submitted).
[45] M. Benmouna, H. Benoit, R. Borsali, M. Duval, *Macromolecules* **1987**, *20*, 2620.
[46] A. Z. Akcasu, R. Klein, B. Hammouda, *Macromolecules* **1993**, *26*, 4136.
[47] N. P. Balsara, P. Stepanek, T. P. Lodge, M. Tirrell, *Macromolecules* **1991**, *24*, 6227.
[48] A. N. Semenov, G. Fytas, S. H. Anastasiadis, *Polym. Prepr. Am. Chem. Soc., Div. Polym. Chem.* **1994**, *35*, 618.
[49] see, for example, A. Halperin, M. Tirrell, T. P. Lodge, *Adv. Polym. Sci.* **1992**, *100*, 33 (and references therein).
[50] Z. Tuzar, P. Kratochvil, in: *Surface and Colloid Science*, Vol. 15, (E. Matijevic, ed.), Plenum, New York, 1993, pp. 1–83.
[51] N. P. Balsara, M. Tirrell, T. P. Lodge, *Macromolecules* **1991**, *24*, 1975.
[52] J. Melenkevitz, M. Muthukumar, *Macromolecules* **1991**, *24*, 4199.

[53] Y. Matsushita, K. Mori, Y. Mogi, R. Saguchi, I. Noda, M. Nagasawa, T. Chang, C. J. Glinka, C. C. Han, *Macromolecules* **1990**, *23*, 4317.
[54] Y. Matsushita, K. Mori, R. Saguchi, I. Noda, M. Nagasawa, T. Chang, C. J. Glinka, C. C. Han, *Macromolecules* **1990**, *23*, 4387.
[55] H. Hasegawa, T. Hashimoto, H. Kawai, T. P. Lodge, E. J. Amis, C. J. Glinka, C. C. Han, *Macromolecules* **1985**, *18*, 67.
[56] K. Almdal, K. A. Koppi, F. S. Bates, K. Mortensen, *Macromolecules* **1992**, *25*, 1743.
[57] I. W. Hamley, K. A. Koppi, J. H. Rosedale, F. S. Bates, K. Almdal, K. Mortensen, *Macromolecules* **1993**, *26*, 5959.
[58] K. A. Koppi, M. Tirrell, F. S. Bates, *Phys. Rev. Lett.* **1993**, *70*, 1449.
[59] K. A. Koppi, M. Tirrell, F. S. Bates, K. Almdal, R. H. Colby, *J. Phys. II France* **1992**, *2*, 1941.
[60] T. Hashimoto, M. Shibayama, H. Kawai, *Macromolecules* **1980**, *13*, 1237.
[61] M. A. Singh, C. R. Harkless, S. E. Nagler, R. F. Shannon, Jr., S. S. Ghosh, *Phys. Rev. B* **1993**, *47*, 8425.
[62] J. W. Cahn, *Acta Metall.* **1956**, *4*, 449.
[63] S. H. Anastasiadis, T. P. Russell, S. K. Satija, C. F. Majkrzak, *J. Chem. Phys.* **1990**, *92*, 5677.
[64] M. D. Foster, M. Sikka, N. Singh, F. S. Bates, S. Satija, C. F. Majkrzak, *J. Chem. Phys.* **1992**, *96*, 8605.
[65] A. J. Liu, G. H. Fredrickson, *Macromolecules* **1992**, *25*, 5551.

Received October 5, 1993. Revision April 7, 1994.